



Investigation of dielectric relaxation behavior, electric modulus and a.c conductivity of low doped polyaniline cadmium oxide (PANI-CdO) nanocomposites

Nadeem Anwar, et al. *[full author details at the end of the article]*

Received: 27 June 2020 / Revised: 19 May 2021 / Accepted: 25 May 2021 /

Published online: 17 July 2021

© The Author(s), under exclusive licence to Springer-Verlag GmbH Germany, part of Springer Nature 2021

Abstract

In situ chemical polymerization method was used to synthesize the polyaniline (PANI) and polyaniline cadmium oxide (PANI-CdO) nanocomposites. The morphology and structure of pure PANI and PANI-CdO nanocomposites were characterized by scanning electron microscopy (SEM) and X-ray diffraction (XRD) analysis, whereas electrical properties were studied by dielectric, electric modulus and a.c conductivity. Various dopant-to-polymer ratios were used to investigate their effect on the characteristics of the synthesized samples. The SEM images exhibited granular as well as flaky structures of PANI and PANI-CdO nanocomposites. The XRD patterns revealed that pure PANI exhibits amorphous nature, while PANI-CdO nanocomposites exhibit polycrystalline nature. The crystallinity and intensity of (XRD) peaks of composite are enhanced by increasing CdO contents. The dielectric measurements show a decrease in dielectric constant, dielectric loss and a decrease in tangent loss with the increase in frequency and nearly constant values at higher frequencies, while the values of dielectric properties increase with the rise in temperature and doping concentration. The electric field modulus was used to analyze the relaxation behavior of the synthesized samples and found to be increased with frequency and decreased with the temperature and CdO concentration. The a.c conductivity was observed to increase with the increase in frequency and temperature for PANI and PANI-CdO composites. The changing behavior of the frequency exponent (S) at various temperatures was analyzed to observe different conduction mechanisms, and a correlated barrier hopping model (CBH) was found to be observed in PANI-CdO composites as well as in pure PANI. The Log a.c conductivity decreases versus the inverse of temperature and with increase in frequency that confirms that the hopping mechanism is the dominant charge transport mechanism.

Keywords Morphology · Composition · Polycrystalline · Nanocomposite · Dielectric

Introduction

In recent years, transition metal oxide (TMO) nanocrystalline II–IV semiconductors have been extensively focused by researchers due to their wide range of applications [1–3]. Cadmium oxide (CdO) is an n-type II–IV semiconductor with a direct band gap of 2.5 eV and an indirect band gap of 1.98 eV. CdO possesses outstanding properties as it has a large number of surface atoms [4–6]. CdO has promising applications in both semiconductor and piezoelectric devices such as photodiodes, solar cells, photo transistors, transparent electrodes, catalysts and gas sensors [7–11].

On the other hand, conducting polymers have a wide range of applications such as sensors by detecting vapor of a variety of gases [12], lightweight batteries [13], Schottky diodes [14], field-effect transistors (FETs) [15] and light-emitting diodes (LEDs) [16]. Among the family of conducting polymers, Polyaniline (PANI) is an extensively used polymer for synthesizing nanocomposites due to its high conductivity, simple synthesis, high compatibility, good thermal and environmental stability, and reversible acid–base chemistry in aqueous solutions [17, 18].

Its chemical formula is $C_6H_5NH_2$ in which a phenyl group C_6H_5 is attached to the amino group NH_2 as shown in Fig. 1. The electrical conductivity of PANI can be modified by the addition of inorganic fillers [19]. Additionally, the electrical conductivity of PANI depends on dopant ions [20–22].

The conducting polymer/inorganic nanocomposites have unique physical and mechanical properties and have attracted much attention from researchers as they combine the merits of conducting polymers and inorganic nanoparticles [23]. Recently, several reports have been published to synthesize PANI/inorganic nanocomposites such as TiO_2 [24–26], CdS [27], silica [28], Ag [29, 30], Na^+ -montmorillonite [31], CeO_2 [32], Fe_3O_4 [33], Zn [34] and MnO_2 [35].

In the present work, a low dopant-to-polymer ratio was used to synthesis the PANI-CdO nanocomposites via In situ chemical polymerization method. The effect of CdO on the dielectric behavior, electric field modulus and a.c conductivity of conducting polyaniline composites has been studied in temperature range 30 °C to 180 °C with an increasing step of 30 °C.

Experimental work

Materials

Aniline was purchased from Riedel-de-Haen. Cadmium oxide (CdO) was purchased from UNI-CHEM chemical reagents, and ammonium persulfate (APS) was provided by Duksan Reagents. Hydrochloric acid (HCl) was purchased from Sacharlu. All the materials were used as received without any further purification except aniline.

Synthesis of polyaniline (PANI) and polyaniline cadmium oxide (PANI-CdO) nanocomposites

In situ chemical polymerization method was used to synthesize polyaniline in open atmosphere, and APS was used as an oxidant. The molar ratio aniline/APS was kept 2:1. For this purpose, 6.125 gm of APS was dissolved in 50 ml distilled water and stirred on magnetic stirrer for 20 min at room temperature. After that 5 ml of aniline was added into 50 ml distilled water separately and 5 ml HCl was added drop wise in order to maintain the pH between 0–1, while the solution was kept on stirring continuously. After half an hour, both the solutions were mixed slowly and further stirred for 3 h. The solution was left over night in open atmosphere to complete the polymerization. Finally, the obtained greenish-black solution was filtered using Whatman filter paper and washed repeatedly with methanol and deionizing water to remove HCl from the solution. The suspension was placed in a vacuum oven at 80 °C to dry and then ground to fine powder [36].

PANI-CdO nanocomposites of (0.5, 1.5 and 2.5) weight percentage of CdO dopant were synthesized by In situ chemical polymerization method. Further steps were the same as that of the synthesis of polyaniline as discussed above.

Measurements

Scanning electron micrographs were obtained by MAIA3 TESCAN instrument having 10.0 kx magnifications. X-rays diffraction patterns were obtained by Bruker model D8 Advanced equipped with Cu K α radiations of wavelength $\lambda = 1.5406 \text{ \AA}$. The instrument was operated at 40 kV and 30 mA, and the diffraction patterns were recorded in the range of 10° to 80° at a scan rate of 2°/min. Two-probe technique was used to characterize the dielectric, a.c conductivity and electric modulus properties of pure and synthesized PANI-CdO nanocomposites in temperature range 30 °C to 180 °C with an increasing step of 30 °C.

These measurements were carried out with the help of G_w INSTRON (LCR) meter Model 8101 and a current source electrometer. The temperature was monitored by FENWAL digital bimetallic thermometer. The reproducibility of every sample was checked thrice.

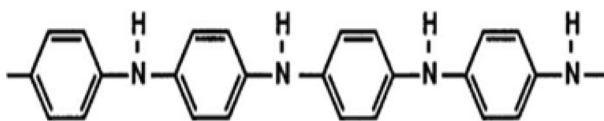


Fig. 1 Chemical structure of polyaniline (PANI)

Results and discussions

SEM investigations

SEM image of pristine CdO shown in Fig. 2e revealed agglomeration of small spherical, spindle, dumbbell and cuboidal-shaped particle crystallites [37]. SEM image of pure PANI shown in Fig. 2a revealed agglomeration and porous morphology as well as flaky structure, whereas SEM images of PANI–CdO nanocomposites (Fig. 2b, c, d) revealed a random distribution of CdO particles into the PANI matrix as well as agglomerates of the fibrous flaky structure of indefinite shapes. This may be attributed to the large surface area of CdO that contributes greater binding sites to the polymer.

XRD Analysis

The XRD pattern of pure PANI Fig. 3a revealed a single characteristic peak at $2\theta = 24.8^\circ$ which represents the amorphous-like structure due to the repetition of benzenoid and quinoid rings in PANI chains [38]. The XRD pattern of pristine CdO Fig. 3e exhibits three sharp diffraction peaks at $2\theta = 40.1^\circ$, 46.6° and 68.2° corresponding to hkl planes (111), (200) and (311), respectively [37]. The observed reflection peaks of CdO are matched with the reference patterns of JCPDS Card No. 05–0640 with monoclinic structure. The XRD patterns of composite samples (Fig. 3b, c, d) also show reflections from (111), (200) and (311) planes at $2\theta = 40.1^\circ$, 46.6° and 68.2° , respectively. No shifting of peaks was observed due to a small fraction of CdO nanoparticles which is less than 3%, but their intensity increases with the increase of CdO in PANI–CdO nanocomposites. The addition of CdO in PANI provides larger surface area to PANI molecules to accumulate on its surface due to which PANI chains have been arranged in greater order. This increase in order between polymer chains suppresses the amorphous nature of PANI and the appearance of CdO peaks in XRD diffractograms indicates an increase in its crystalline nature. The syntheses of both metal oxide and PANI conducted simultaneously, resulting in a uniform distribution of the metal oxide over the PANI network [39]. Another approach is that the metal oxide can be used as the oxidizing agent for initiating the polymerization process [40]. In this case, the PANI is directly grown from the metal oxide, and thus, forming a strong interaction with the metal oxide at a nanoscale. So PANI grows well on its surface and PANI chains may arrange in regular pattern. That is why peaks of CdO become more intense on increasing the weight percentage of CdO in PANI/CdO composites. The increase in peak intensity can be attributed to increase in crystallinity of PANI/CdO composite. The crystallinity of synthesized samples was calculated by XRD (WAXS) formula [41]. The crystallite sizes were calculated by Debye–Scherrer’s formula for (111), (200) and (311) planes [42] as shown in Table 1.

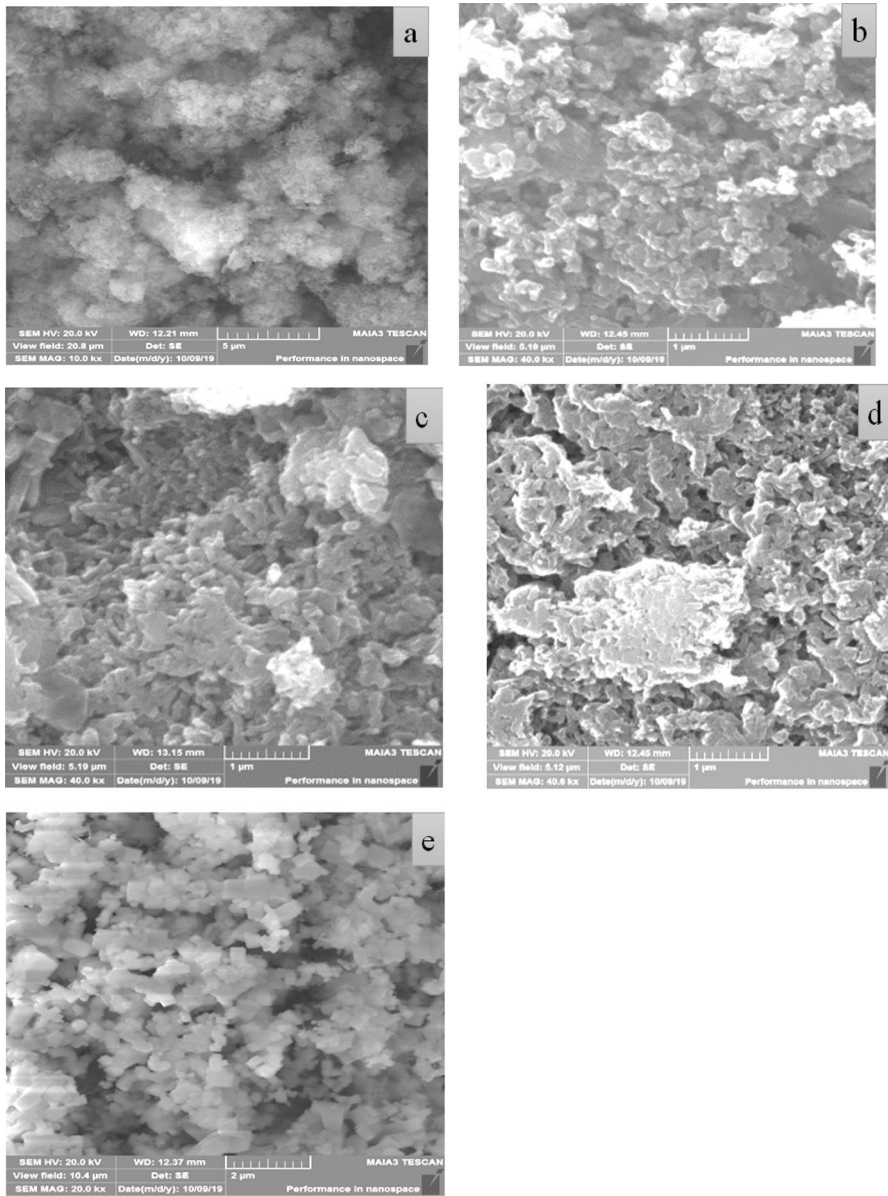


Fig. 2 SEM images of **a** pure PANI, **b** PANI-0.5%CdO, **c** PANI-1.5%CdO, **d** PANI-2.5%CdO and **e** pristine CdO, respectively

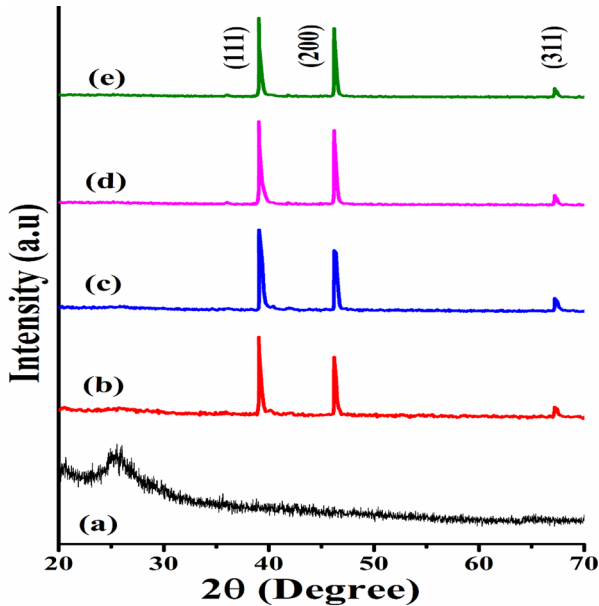


Fig. 3 XRD patterns of **a** pure PANI, **b** PANI-0.5%CdO, **c** PANI-1.5%CdO, **d** PANI-2.5%CdO, **e** pristine CdO, respectively

Dielectric behavior of PANI and PANI-CdO nanocomposites

Effect of frequency, temperature and CdO concentration on dielectric constant

Figure 4 represents the dielectric constant (ϵ') as a function of frequency ranging from 1 Hz to 1 MHz for PANI and PANI-CdO nanocomposites at room and elevated temperatures. The dielectric constant (ϵ') was observed to vary with frequency, temperature and filler concentration. The dielectric constant (ϵ') has higher values at lower frequencies and decreases sharply as frequency increases and becomes nearly constant as the frequency approaches to higher values. The dielectric constant (ϵ') is given by Eq. (1)

$$\epsilon' = Cd/A\epsilon_0$$

where C is the capacitance, d is the thickness of the pellet, A is the area of the pellet, and ϵ_0 is the free space permittivity.

It was also observed that the dielectric constant (ϵ') increases with the rise in temperature and filler CdO concentration and becomes nearly constant at higher temperatures. As the temperature rises, the intermolecular forces between the polymer chains are broken which cause an increase in thermal agitation. This heating treatment affects the dipoles polarization by reducing the relaxation time, and polymer chains prefer to align in phase with the changing frequency and contribute to enhancing the dielectric constant [43].

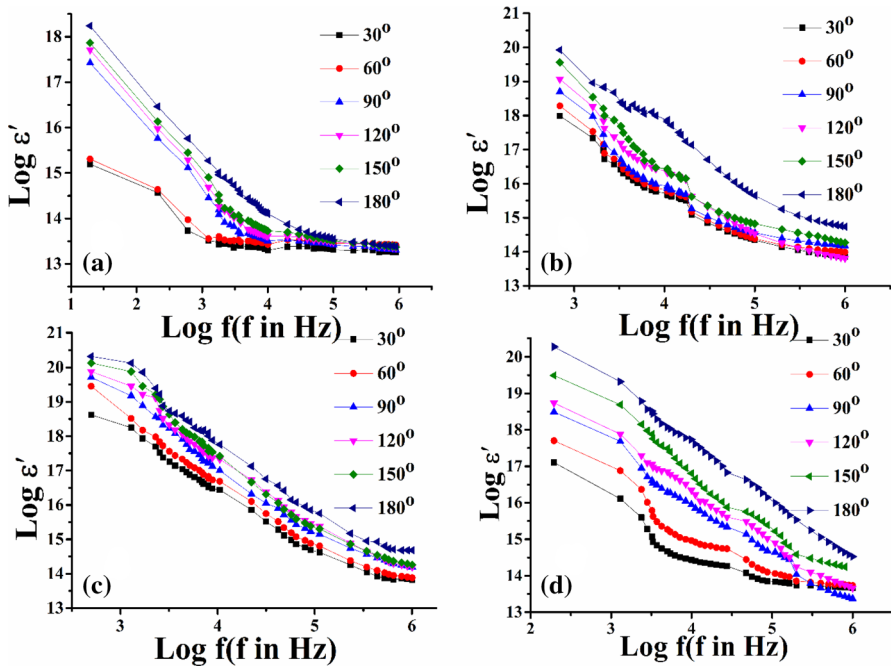


Fig. 4 Log ϵ' vs Log f a pure PANI, b PANI-0.5%CdO, c PANI-1.5%CdO, d PANI-2.5%CdO, respectively

Effect of frequency, temperature and CdO concentration on dielectric loss

Dielectric loss (ϵ'') is expressed in Eq. (2)

$$\epsilon'' = \epsilon' \tan \delta$$

The above relation shows that the dielectric loss is directly proportional to the dielectric constant so satisfies the same results as for the dielectric constant.

Figures 4 and 5 show that (ϵ') and (ϵ'') have higher values at lower frequencies and decrease with the rise in frequency for all temperature [44]. This increase in (ϵ') and (ϵ'') at low frequencies is also characterized by the deposition of additional charge carriers at the interfaces, which may increase the net dipoles on the interface. This increase in electrical dipoles may play a crucial role to change the net polarization of the ionic medium that helps to boost the dielectric constant (ϵ'). However, as the frequency approaches to higher values, the dipoles do not have enough relaxation time to follow the applied electrical field. Therefore, surface polarization is expected to decrease which results in the reduction of (ϵ') and (ϵ'') values. At higher frequency, atomic or electronic polarization typically happens [45].

Figures 4 and 5 show that the values of (ϵ') and (ϵ'') are low for lower temperatures and lower concentration of CdO in PANI and increase with the increase in content of CdO in PANI at the lower end of frequency and gradually decrease as

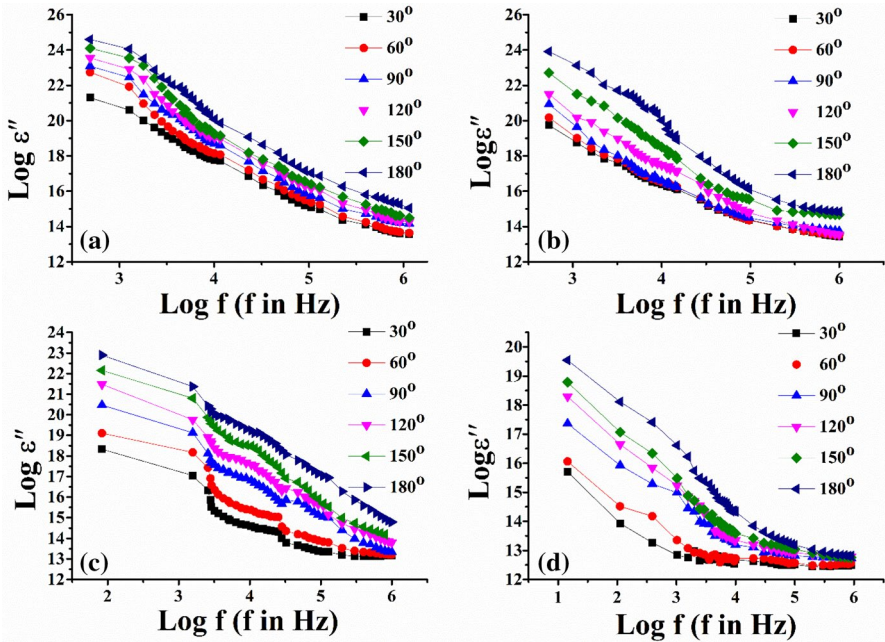


Fig. 5 Log ϵ'' vs Log f a pure PANI, b PANI-0.5%CdO, c PANI-1.5%CdO, d PANI-2.5%CdO, respectively

frequency approaches to higher values. Both (ϵ') and (ϵ'') display strong scattering toward the lower frequency end which may built up space charge polarization along with non-negligible ionic conductivity due to the accumulation of charge carriers at the interface between the sample and the electrodes. At high frequencies, the charge deposition is minimal at the interface; therefore, (ϵ') and (ϵ'') are relatively constant and the charge carriers neglect to respond to the external electric field which leads to lattice polarization. This accounts for a linear decrease in the (ϵ') and (ϵ'') values at a low-frequency region and a frequency-independent plateau region at high frequencies.

The dielectric behavior described by the complex permittivity ϵ^* gives the information about the charge transport mechanism in the system and is given by Eq. (3)

$$\epsilon^* = \epsilon' - i\epsilon''$$

where ϵ' is storage energy and ϵ'' is the loss of energy in each cycle of applied electric field. At low frequencies for all temperatures, relative permittivity has higher values, whereas at higher frequencies, the values of relative permittivity are nearly constant [46]. This increase in dielectric constant and loss is related to the localized mobile charges that may contribute to the formation of interfacial dipoles due to electric polarization. At higher values of frequencies, dipoles do not have enough

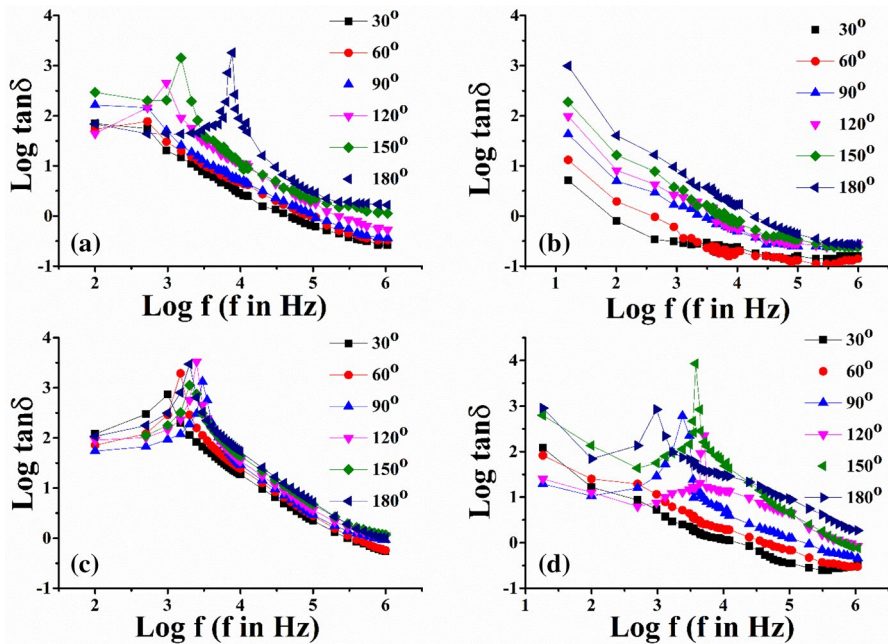


Fig. 6 Log tan δ vs Log f **a** pure PANI, **b** PANI-0.5%CdO, **c** PANI-1.5%CdO, **d** PANI-2.5%CdO, respectively

relaxation time (T_r) to be aligned along the field and do not depend upon frequency. The frequency-independent values are known as (ϵ'_s) static dielectric constant. [47]. At low frequencies, dipoles have ample time to arrange themselves in the direction of the applied electric field and frequency-dependent behavior is observed. At ($f < f_r = 1/2\pi T_r$), dipoles follow the field in each dispersion region, where f_r is mean relaxation frequency and $\epsilon'_r = \epsilon'_s$. The mechanism which contributes to the dielectric properties may be attributed to the interaction of electric field with electronic, interfacial, dipolar and atomic polarization [48]. This may also be because of the charge transport mechanism at the valance states of cations [49].

With increase in frequency, the dipoles do not follow the field and lag behind according to their mobility which results in a slight decrease of ϵ'_r . After relaxation frequency $f_r = 1/2\pi T_r$ (T_r is relaxation time), the dipoles are not able to follow the applied electric field so a sharp decrease in (ϵ') and (ϵ'') was observed. The higher values of (ϵ') and (ϵ'') at the lower end of frequency as compared to higher-frequency end may be ascribed to all types of polarization such as an electrode, interfacial, dipolar, atomic, ionic and electronic contributions. The higher values of (ϵ') and (ϵ'') at lowered frequencies may be attributed to Maxwell–Wagner polarization [50, 51] in heterogeneous systems. Maxwell–Wagner surface polarization model [52] is confirmed by the reduction in dielectric constant with increase in frequency. So, our results are in good agreement with the literature [47, 48]. Results shown in Table 2.

Frequency and temperature dependences of tangent loss

The loss of energy in an insulating material can be measured by the phase (δ) relation of current and applied voltage as

$$D(\omega) = \tan \delta = \epsilon'' / \epsilon'$$

where $\delta = 90^\circ - \theta$ and θ is the phase angle.

In insulating materials, the applied electric field $E(\omega)$ leads ahead to loss tangent $D(\omega)$ by an angle (δ) that causes the energy dissipation. The deviation of $D(\omega)$ from 90° is called the dielectric loss factor. The decrease in tangent loss with increase in frequency at different temperatures is a typical characteristic of conjugated compounds. Hence, our results sensibly follow the literature as shown in Fig. 6 [53, 54].

Electric modulus spectra

The electric modulus represents the real dielectric relaxation process and is defined as the inverse of permittivity which is used to analyze ionic conductivities.

$$M^* = (\epsilon^*)^{-1} = M' + iM'' \quad (5)$$

where M' and M'' are the real and imaginary components defined as

$$M' = \epsilon' (\epsilon'^2 + \epsilon''^2)^{-1} \quad (6)$$

$$M'' = \epsilon'' (\epsilon'^2 + \epsilon''^2)^{-1} \quad (7)$$

The values of both M' and M'' are approaching zero at a low frequency due to a slight contribution of electrode polarization and approaches to the highest values at higher frequencies due to the relaxation process. This can be attributed to the long-range mobility of charge carriers. The M'' part represents the hopping of ions from one site to a neighboring site at low frequency, whereas the peaks at high frequencies represent the segmental and ionic conduction. The M' and M'' spectra of pure and nanocomposites at various temperatures in Figs. 7 and 8 show that M' and M'' values reduce with the temperature rise, while the peaks of M' and M'' spectra show a significant rise in its height with a shift toward the high frequency region which corresponds to reduction with increase in temperature. This reduction contributes to the better flexibility of the polymeric matrix, as these peaks move toward higher-frequency region under rising temperature. Such shifts may be originated from the accumulation of free charges at the interface with the rise in temperature. Thus, the relaxation time decreases with the increase in charge carrier mobility. The shifting of peaks toward the higher-frequency region with the temperature rise indicates that the relaxation process is thermally activated, and the hopping mechanism of charge carriers is dominated intrinsically.

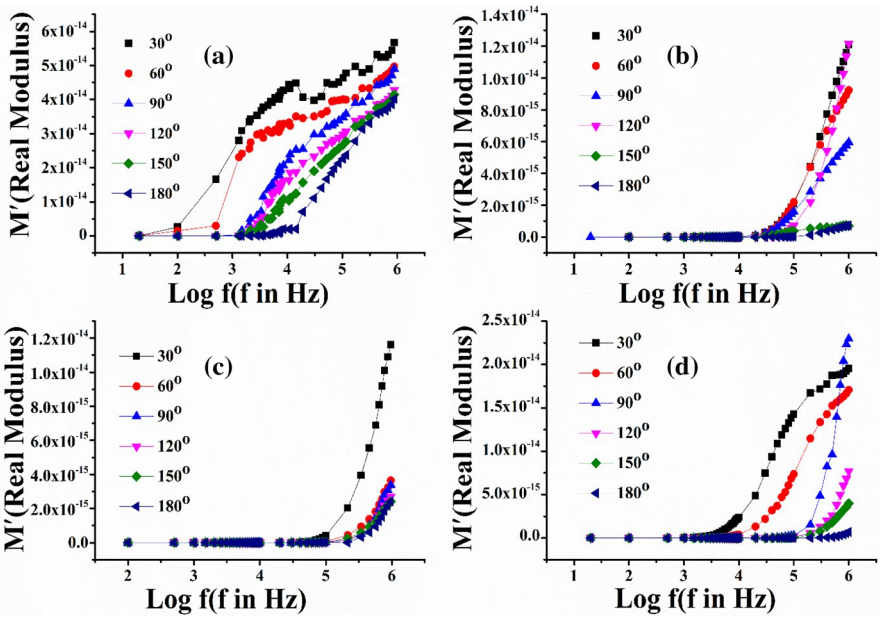


Fig. 7 M' vs $\text{Log } f$ a Pure PANI, b PANI-0.5%CdO, c PANI-1.5%CdO, d PANI-2.5%CdO, respectively

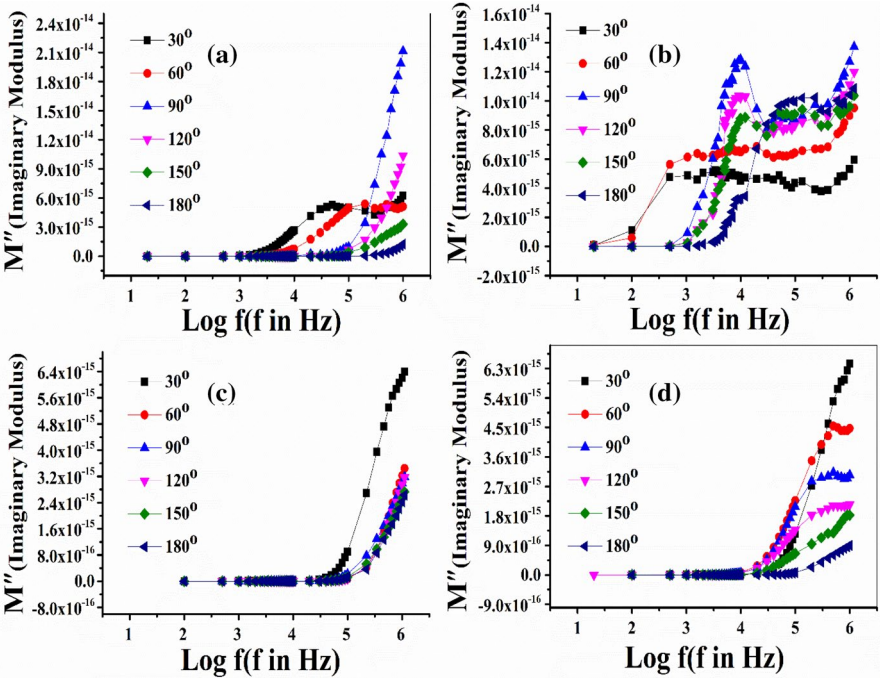


Fig. 8 M'' vs $\text{Log } f$ a Pure PANI, b PANI-0.5%CdO, c PANI-1.5%CdO, d PANI-2.5%CdO, respectively

In Figs. 7 and 8, the peaks are shifted toward a higher-frequency region under the increase in concentration of CdO nanoparticles, indicating that the relaxation time decreases as the dopant concentration increases.

a.c Conductivity $\sigma_{a.c}(\omega)$

a.c conductivity of polymeric composites is usually associated with polymer's polarity and the filler particles conductivity, its crystallinity and the structure of electric network among the filler and the polymer chains. a.c conductivity of a material is given by Eq. (8 and 9) [55]

$$\sigma_{a.c}(\omega) = \omega \epsilon_0 \epsilon'' \tan \delta \quad (8)$$

$$\sigma_{a.c}(\omega) = 2\pi f \epsilon_0 \epsilon'' \tan \delta \quad (9)$$

The above relation shows that ($\sigma_{a.c}$) increases with the rise in frequency; Maxwell–Wagner model has explained this frequency-dependent behavior [51, 52]. Figure 9 shows considerable change in conductivity of prepared samples with the

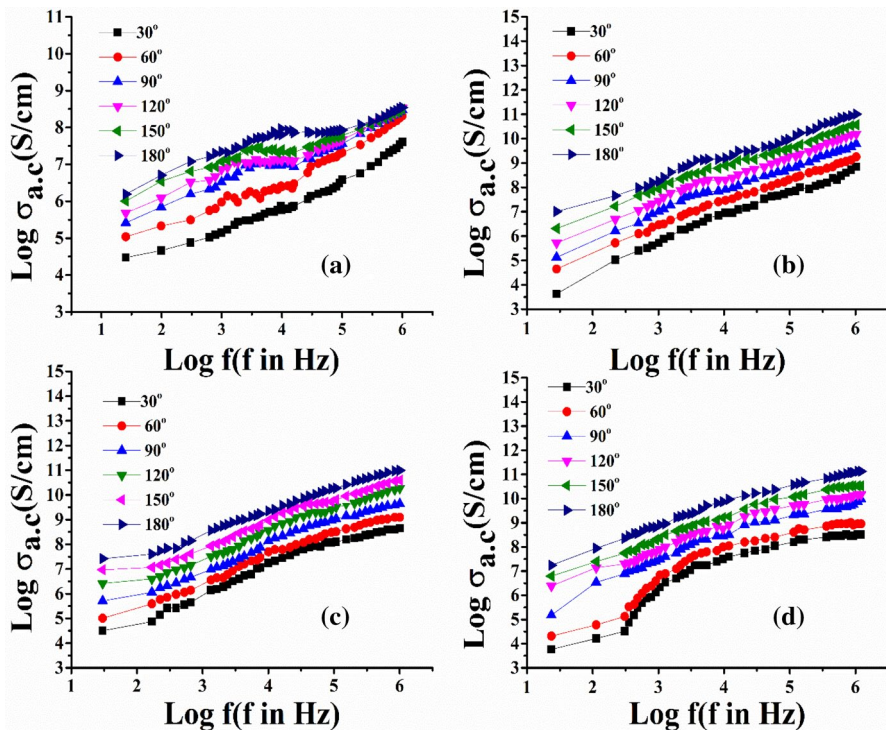


Fig. 9 Log $\sigma_{a.c}$ vs Log f a pure PANI, b PANI-0.5%CdO, c PANI-1.5%CdO, d PANI-2.5%CdO, respectively

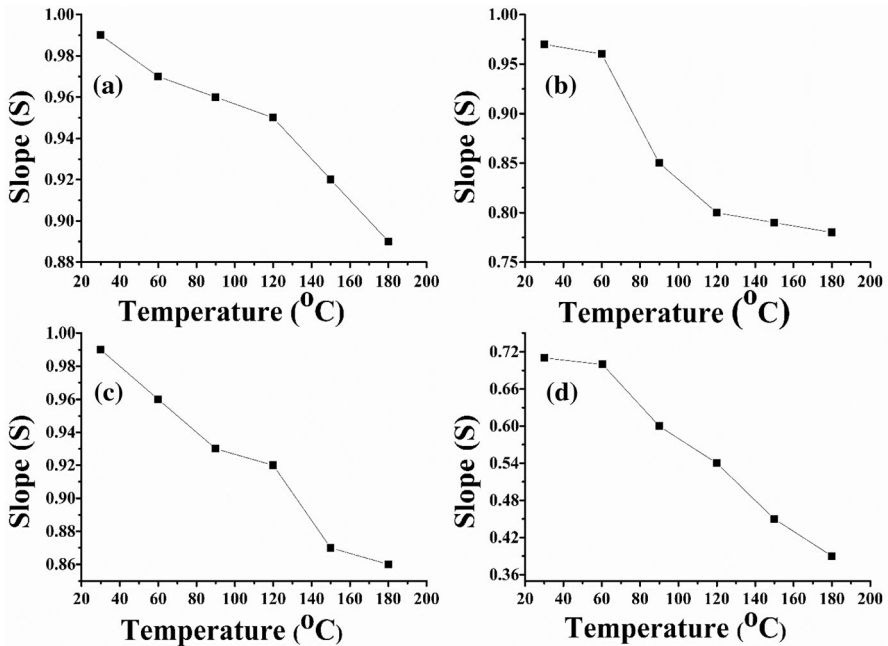


Fig. 10 Slope (S) vs Temperature (°C) **a** pure PANI, **b** PANI-0.5%CdO, **c** PANI-1.5%CdO, **d** PANI-2.5%CdO, respectively

change in frequency of the applied electric field, temperature, and concentration of CdO. The bonds begin to rotate with available flexible polar bonds in polymer chains at higher frequencies; therefore, a.c conductivity increases with increase in frequency.

The frequency-dependent conductivity $\sigma_{a.c}(\omega)$ of disordered solid materials such as PANI-CdO nanocomposites can be approximated by an empirical law named as “universal power law” by Jonscher [56].

$$\sigma_{a.c}(\omega, T) = A(T)\omega^S \tag{10}$$

where A is a pre-exponential factor, ω is the angular frequency, and S is frequency exponent $0 < S < 1$. For frequency-independent or dc electrical conduction $S=0$ and frequency-dependent or a.c electrical conduction $S \leq 1$.

Models for frequency(f) and temperature (T) dependency of slope (S)

There are several theoretical models to explain the conduction mechanism of materials depending upon S. If S is being frequency dependent and independent of temperature, then it follows the quantum tunneling model (QMT). If S is predicted to depend both upon frequency and temperature but increases with the temperature rise, then it follows small polaron tunneling model (SPT) [57]. If S depends both on temperature as well as on frequency and decreases first then

Table 1 hkl plane, 2θ (degree), d_{hkl} (Å), D (nm), %age crystallinity of pure PANI, PANI-0.5%CdO, PANI-1.5%CdO, PANI-2.5%CdO, pristine CdO, respectively, with ± 0.5 uncertainty

Sample	hkl plane	2θ (degree)	Calculated d_{hkl} (Å)	D (nm)	%age crystallinity
Pure PANI					53
PANI-0.5%CdO	111	40.1	2.24	0.44	68.5
	200	46.6	1.94	0.43	
	311	68.1	1.37	0.37	
PANI-1.5%CdO	111	40.1	2.24	0.44	77.5
	200	46.6	1.94	0.43	
	311	68.1	1.37	0.37	
PANI-2.5%CdO	111	40.1	2.24	0.44	78.5
	200	46.6	1.94	0.43	
	311	68.1	1.37	0.37	
Pristine CdO	111	40.1	2.24	0.44	98.5
	200	46.6	1.94	0.43	
	311	68.1	1.37	0.37	

increases with the temperature rise, so it follows the large polaron tunneling model (LPT) [58], and if S depends both on temperature and frequency and decreases with the temperature rise, then it follows correlated barrier hopping model (CBH) [59]. In our case, the correlated barrier hopping model (CBH) [60, 61] behavior of S is dominant, which has already been reported by other workers [62]. In the CBH model, the conduction takes place via bipolaron hopping process in which two polarons simultaneously hop over the potential barrier between two charged defect states and barrier height is correlated with the inter-site separation via a coulombic interaction.

The frequency exponent S is given by the expression [63]

$$S = 1 - (6K_B T/W) \quad (11)$$

where K_B is Boltzmann constant, T is absolute temperature, and W is the barrier height which is the energy required to take two electrons from the charged defect sites.

Equation (11) can be arranged as

$$1 - S = 6K_B T/W \quad (12)$$

From the values of S (Fig. 10), W has been calculated by using Eq. (12) for our synthesized samples. The values of W found are shown in Table 2. It has been found that the barrier height decreases with increase in temperature and increase in concentration of dopant CdO. The obtained value of W is related to the optical band gap of the material [64].

Table 2 The observed average dielectric constant, dielectric loss and tangent loss of pure PANI, PANI-0.5%CdO, PANI-1.5%CdO, PANI-2.5%CdO and pristine CdO composites at different temperatures

Sr. No	Material	Temperature (°C)	Average dielectric Constant (ϵ')	Average dielectric Loss (ϵ'')	Average tangent Loss D(ω)	Barrier Height (eV)
1	Pure PANI	30°	6.8×10^5	3.3×10^5	0.51	0.1324
		60°	7.8×10^5	3.8×10^5	0.51	0.0441
		90°	9.5×10^5	7.1×10^5	0.78	0.0331
		120°	1.0×10^6	8.9×10^5	0.84	0.0264
		150°	1.1×10^6	1.0×10^6	0.92	0.0165
		180°	1.5×10^6	1.8×10^6	1.18	0.0120
2	PANI-0.5%CdO	30°	1.7×10^6	1.6×10^6	1.02	0.1324
		60°	2.5×10^6	3.0×10^6	1.26	0.0331
		90°	4.4×10^6	8.7×10^6	1.93	0.0189
		120°	6.2×10^6	1.6×10^6	2.38	0.0101
		150°	1.1×10^7	3.7×10^7	4.10	0.0094
		180°	2.1×10^7	7.9×10^7	3.85	0.0045
3	PANI-1.5%CdO	30°	4.3×10^6	6.7×10^6	1.38	0.0440
		60°	4.8×10^6	7.4×10^6	1.59	0.0331
		90°	5.6×10^6	8.6×10^6	1.72	0.0088
		120°	6.9×10^6	1.5×10^7	2.30	0.0066
		150°	9.0×10^6	3.9×10^7	2.71	0.0063
		180°	2.3×10^7	1.1×10^8	3.62	0.0060
4	PANI-2.5%CdO	30°	7.6×10^6	2.0×10^7	2.79	0.0044
		60°	9.7×10^6	2.9×10^7	3.10	0.0033
		90°	1.5×10^7	5.3×10^7	3.45	0.0028
		120°	1.8×10^7	7.2×10^7	3.76	0.0024
		150°	2.0×10^7	1.0×10^8	3.89	0.0021
		180°	2.8×10^7	2.2×10^8	4.18	0.0013

The straight lines of $\text{Log } \sigma_{a.c}$ with the inverse of temperature follow the Arrhenius equation:

$$\sigma_{a.c} = \sigma_0 e^{-Ea.c/K_B T} \tag{13}$$

where σ_0 is the pre-exponential constant and Ea.c is the activation energy.

The activation energies of our synthesized samples were calculated from the slope of the straight lines of Fig. 11. This shows that $\text{Log } \sigma_{a.c}$ conductivity decreases with inverse of temperature and with increase in frequency; this can be attributed to enhancing the electronic jumps between the localized states under applied field frequency. This confirms that the hopping charge transport mechanism is dominant in our synthesized samples. Our present result is in

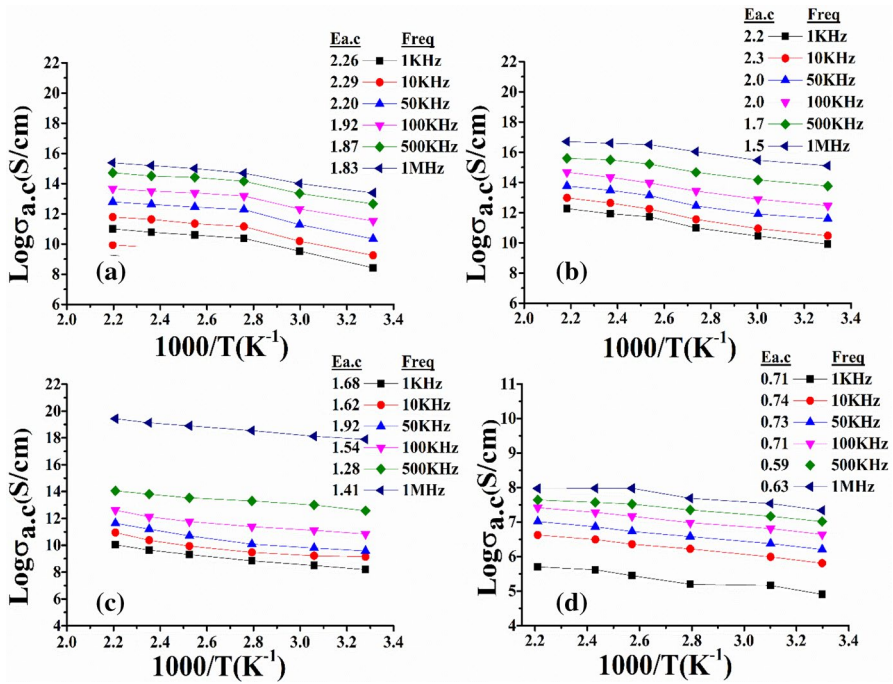


Fig. 11 $\text{Log } \sigma_{a.c.}$ vs $1000/T$ **a** pure PANI, **b** PANI-0.5%CdO, **c** PANI-1.5%CdO, **d** PANI-2.5%CdO, respectively

good agreement with the recently reported results for other amorphous materials [65–67]

Conclusion

In situ chemical polymerization method was used to synthesize the polyaniline (PANI) and polyaniline cadmium oxide (PANI-CdO) nanocomposites. The morphology and structure of pure PANI and PANI-CdO nanocomposites were characterized by scanning electron microscopy (SEM) and X-ray diffraction (XRD) analysis, whereas electrical properties were studied by dielectric, electric modulus and a.c conductivity. Various dopant-to polymer-ratios were used to investigate their effect on the characteristics of the synthesized samples. The SEM images exhibited granular as well as flaky structures of PANI and PANI-CdO nanocomposites. The XRD patterns revealed that pure PANI exhibits amorphous nature while PANI-CdO nanocomposites exhibit polycrystalline nature. The crystallinity and intensity of (XRD) peaks of composite are enhanced by increasing CdO contents. The dielectric measurements show a decrease in dielectric constant, dielectric loss and a decrease in tangent loss with the increase in frequency and nearly constant values at higher frequencies, while the values of dielectric properties increase with the rise in temperature and doping concentration. The electric field modulus was used to analyze

the relaxation behavior of the synthesized samples and found to be increased with frequency and decreased with the temperature and CdO concentration. The a.c conductivity was observed to increase with the increase in frequency and temperature for PANI and PANI-CdO composites. The changing behavior of the frequency exponent (S) at various temperatures was analyzed to observe different conduction mechanisms, and a correlated barrier hopping model (CBH) was found to be observed in PANI-CdO composites as well as in pure PANI. The Log a.c conductivity decreases versus the inverse of temperature and with increase in frequency that confirms that the hopping mechanism is the dominant charge transport mechanism.

References

1. Parker ID (1994) Carrier tunneling and device characteristics in polymer light-emitting diodes. *J Appl Phys* 75:1656–1666. <https://doi.org/10.1063/1.356350>
2. Jeon H, Ding J, Nurmikko AV, Xie W, Grillo DC, Kobayashi M, Gunshor RL, Hua GC, Otsuka N (1992) Blue and green diode lasers in ZnSe-based quantum wells. *Appl Phys Lett* 60:2045–2047. <https://doi.org/10.1063/1.107109>
3. Rolo AG, Vieira LG, Gomes MJM, Ribeiro JL, Belsley MS, Santos MP (1998) Growth and characterisation of cadmium sulphide nanocrystals embedded in silicon dioxide films. *Thin Solid Films* 312:348–353. [https://doi.org/10.1016/S0040-6090\(97\)00233-2](https://doi.org/10.1016/S0040-6090(97)00233-2)
4. Manickathai K, Viswanathan SK, Alagar M (2008) Synthesis and characterization of CdO and CdS nanoparticles. *Indian J Pure App Phys* 46:561–564. <https://www.researchgate.net/publication/279548537>
5. Majid A, Afza Z, Mutaza S, Nabi G, Ahmad N (2013) Synthesis and characterization of silver doped cadmium oxide nanoparticles. *J Adv Phys* 02:116–118. <https://doi.org/10.1166/jap.2013.1058>
6. Kondawar S, Mahore R, Dahegaonkar A, Agrawal S (2011) Electrical conductivity of cadmium oxide nanoparticles embedded polyaniline nanocomposites. *Adv App Sci Res* 2:401–406. <https://www.pelagiaresearchlibrary.com>
7. Heidari A, Brown C (2015) Study of composition and morphology of cadmium oxide (Cdo) nanoparticles for eliminating cancer cells. *J Nanomed Res* 2:1–20. <https://doi.org/10.15406/jnmr.2015.02.00042>
8. Ferro R, Rodriguez JA (2000) Influence of F-doping on the transmittance and electron affinity of CdO thin films suitable for solar cells technology. *Energy Mater Sol Cells* 64:363–370. [https://doi.org/10.1016/S0927-0248\(00\)00228-2](https://doi.org/10.1016/S0927-0248(00)00228-2)
9. Li J, Ni YH, Liu J, Hong J (2009) Preparation, conversion, and comparison of the photocatalytic property of Cd(OH)₂, CdO, CdS and CdSe. *J Phys Chem Solids* 70:1285–1289. <https://doi.org/10.1016/j.jpcs.2009.07.014>
10. Liu Y, Zhang YC, Xu XF (2009) Hydrothermal synthesis and photocatalytic activity of CdO₂ nanocrystals. *J Hazard Mater* 163:1310–1314. <https://doi.org/10.1016/j.jhazmat.2008.07.101>
11. Lu HB, Liao L, Li JC, Wang DF, He H, Fu Q, Xu L, Tian Y (2006) High surface-to-volume ratio ZnO microberets: low temperature synthesis, characterization, and photoluminescence. *J Phys Chem B* 110:23211–23214. <https://doi.org/10.1021/jp064079r>
12. Laranjeira JMG, Khoury HJ, de Azevedo WM, da Silva Jr EF, da Vasconcelos EA (2002) A silicon-polymer heterostructure for sensor applications. *Braz J Phys* 32:421–423. <https://doi.org/10.1590/S0103-97332002000200050>
13. Kalaycioglu E, Akbulut U, Toppare L (1996) Conducting composites of polypyrrole with polytetramethylbisphenol a carbonate. *J Appl Polym Sci* 61:1067–1075. [https://doi.org/10.1002/\(SICI\)1097-4628\(19960815\)61:7<1067::AID-APP1>3.0.CO;2-K](https://doi.org/10.1002/(SICI)1097-4628(19960815)61:7<1067::AID-APP1>3.0.CO;2-K)
14. Koezuka H, Tsumura A (1989) Field-effect transistor utilizing conducting polymers. *Synth Met* 28:C-753–760. [https://doi.org/10.1016/0379-6779\(89\)90600-0](https://doi.org/10.1016/0379-6779(89)90600-0)

15. Gustafsson G, Treacy GM, Cao Y, Klavetter F, Colaneri N, Heeger AJ (1993) The “plastic” led: A flexible light-emitting device using a polyaniline transparent electrode. *Synth Met* 57:4123–4127. [https://doi.org/10.1016/0379-6779\(93\)90568-H](https://doi.org/10.1016/0379-6779(93)90568-H)
16. Chiang JC, Macdiarmid AG (1986) ‘Polyaniline’: Protonic acid doping of the emeraldine form to the metallic regime. *Synth Met* 13:193–205. [https://doi.org/10.1016/0379-6779\(86\)90070-6](https://doi.org/10.1016/0379-6779(86)90070-6)
17. Gustafsson G, Cao Y, Treacy GM, Klavetter F, Colaneri N, Heeger AJ (1992) Flexible light-Emitting diodes from soluble conducting polymers. *Nature* 357:477–479. <https://doi.org/10.1038/357477a0>
18. Sailor MJ, Ginsburg EJ, Gorman CB, Kumar A, Grubbs RH, Lewis NS (1990) Thin films of n-Si/Poly-(CH₃)₃Si-Cyclooctatetraene: conducting-polymer solar cells and layered structures. *Science* 249:1146–1149. <https://doi.org/10.1126/science.249.4973.1146>
19. Li L, Jiang J, Xu F (2007) Synthesis and ferrimagnetic properties of novel Sm-substituted LiNi ferrite–polyaniline nanocomposite. *Mater Lett* 61:1091–1096. <https://doi.org/10.1016/j.matlet.2006.06.061>
20. Ayad MM, Zaki EA (2008) Doping of polyaniline films with organic sulfonic acids in aqueous media and the effect of water on these doped films. *Eur Polymer J* 44:3741–3747. <https://doi.org/10.1016/j.eurpolymj.2008.08.012>
21. Chung SF, Wen TC, Gopalan A (2005) Influence of dopant size on the junction properties of polyaniline. *Mater Sci Eng B* 116:125–130. <https://doi.org/10.1016/j.mseb.2004.09.023>
22. Long Y, Chen Z, Wang N, Li J, Wan M (2004) Electronic transport in PANI-CSA/PANI-DBSA polyblends. *Phys B: Condens Matter* 344:82–87. <https://doi.org/10.1016/j.physb.2003.09.245>
23. Roy AS, Anilkumar KR, Ambika Prasad MVN (2012) Studies of AC conductivity and dielectric relaxation behavior of CdO-doped nanometric polyaniline. *J Appl Polymer Sci* 123:1928–1934. <https://doi.org/10.1002/app.34696>
24. Xu JC, Liu WM, Li HL (2005) Titanium dioxide doped polyaniline. *Mater Sci Eng C* 25:444–447. <https://doi.org/10.1016/j.msec.2004.11.003>
25. Mo TC, Wang HW, Chen SY, Yeh YC (2008) Synthesis and dielectric properties of polyaniline/titanium dioxide nanocomposites. *Ceram Int* 34:1767–1771. <https://doi.org/10.1016/j.ceramint.2007.06.002>
26. Shi L, Wang X, Lu L, Yang X, Wu X (2009) Preparation of TiO₂/polyaniline nanocomposite from a lyotropic liquid crystalline solution. *Synth Met* 159:2525–2529. <https://doi.org/10.1016/j.synthmet.2009.08.056>
27. Jia W, Segal E, Kornemandel D, Lamhot Y, Narkis M, Siegmann A (2002) Polyaniline–DBSA/organophilic clay nanocomposites: synthesis and characterization. *Synth Met* 128:115–120. [https://doi.org/10.1016/S0379-6779\(01\)00672-5](https://doi.org/10.1016/S0379-6779(01)00672-5)
28. Liu P (2008) Preparation and characterization of conducting polyaniline/silica nanosheet composites. *Mater Sci* 12:9–13. <https://doi.org/10.1016/J.COSSMS.2009.01.001>
29. Jing S, Xing S, Yu L, Wu Y, Zhao C (2007) Synthesis and characterization of Ag/polyaniline core-shell nanocomposites based on silver nanoparticles colloid. *Mater Lett* 61:2794–2797. <https://doi.org/10.1016/j.matlet.2006.10.032>
30. Khanna PK, Singh N, Charan S, Visawanath AK (2005) Synthesis of Ag/polyaniline nanocomposite via an in situ photo-redox mechanism. *Mater Chem Phys* 92:214–219. <https://doi.org/10.1016/j.matchemphys.2005.01.011>
31. Kim BH, Jung JH, Kim JW, Choi HJ, Joo J (2001) Physical characterization of polyaniline–Na⁺–montmorillonite nanocomposite intercalated by emulsion polymerization. *Synth Met* 117:115–118. [https://doi.org/10.1016/S0379-6779\(00\)00549-X](https://doi.org/10.1016/S0379-6779(00)00549-X)
32. He Y (2005) Synthesis of polyaniline/nano-CeO₂ composite microspheres via a solid-stabilized emulsion route. *Mater Chem Phys* 92:134–137. <https://doi.org/10.1016/j.matchemphys.2005.01.033>
33. Xue W, Fang K, Qiu H, Li J, Mao W (2006) Electrical and magnetic properties of the Fe₃O₄–polyaniline nanocomposite pellets containing DBSA-doped polyaniline and HCl-doped polyaniline with Fe₃O₄ nanoparticles. *Synth Met* 156:506–509. <https://doi.org/10.1016/j.synthmet.2005.06.021>
34. Olad A, Barati M, Shirmohammadi H (2011) Conductivity and anticorrosion performance of polyaniline/zinc composites: investigation of zinc particle size and distribution effect. *Prog Org Coat* 72:599–604. <https://doi.org/10.1016/j.porgcoat.2011.06.022>
35. Zhang X, Ji L, Zhang S, Yang W (2007) Synthesis of a novel polyaniline-intercalated layered manganese oxide nanocomposite as electrode material for electrochemical capacitor. *J Power Sources* 173:1017–1023. <https://doi.org/10.1016/j.jpowsour.2007.08.083>

36. Shakoor A, Anwar H, Rizvi TZ (2008) Structural and electrical properties of doped polypyrrole and its composite with montmorillonite clay. *J Compos Mater* 42:2101–2109. <https://doi.org/10.1134/S0965545X1304010X>
37. Zargar RA, Chackarabarti S, Arora M, Hafiz AK (2016) Synthesis, characterization and interpretation of screen-printed nanocrystalline CdO thick film for optoelectronic applications. *Int Nano Lett* 6:99–104. <https://doi.org/10.1007/s40089-015-0172-5>
38. Xingwei L, Wang G, Xiaoxuan L, Dongming L (2004) Surface properties of polyaniline/nano-TiO₂ composites. *Appl Surf Sci* 229:395–401. <https://doi.org/10.1016/j.apsusc.2004.02.022>
39. Zheng L, Xu Y, Jin D, Xie Y (2011) Polyaniline-intercalated molybdenum oxide nanocomposites: simultaneous synthesis and their enhanced application for supercapacitor. *Chem Asian J* 6:1505–1514. <https://doi.org/10.1002/asia.201000770>
40. Jaidev RI, Jafri AK, Mishra SR (2011) Polyaniline–MnO₂ nanotube hybrid nanocomposite as supercapacitor electrode material in acidic electrolyte. *J Mater Chem* 21:17601–17605. <https://doi.org/10.1039/C1JM13191E>
41. Bragg WL (1913) The diffraction of short electromagnetic waves by a crystal. *Proc Cambridge Philos Soc* 17:43–57
42. Patterson AL (1939) The scherrer formula for X-ray particle size determination. *Phys Rev American Phys Soc* 56:978–982. <https://link.aps.org/doi/10.1103/PhysRev.56.978>
43. Ahmad Z (2012) Polymer dielectric materials. In: *Dielectric Material*. University Sains Malaysia, pp 3–26. <https://doi.org/10.5772/50638>
44. Psarras GC (2006) Hopping conductivity in polymer matrix–metal particles composites. *Compos Part A Appl Sci Manuf* 37:1545–1553. <https://doi.org/10.1016/j.compositesa.2005.11.004>
45. Wang L, Dang ZM (2005) Carbon nanotube composites with high dielectric constant at low percolation threshold. *Appl Phys Lett* 87(1–3):042903. <https://doi.org/10.1063/1.1996842>
46. Pinto NJ, Sinha GP, Aliev FM (1998) Frequency-dependent conductivity and dielectric permittivity of emeraldine base and weakly doped poly(o-toluidine). *Synth Met* 94:199–203. [https://doi.org/10.1016/S0379-6779\(98\)00003-4](https://doi.org/10.1016/S0379-6779(98)00003-4)
47. Patankar KK, Dombale PD, Mathe VL, Patil SA, Patil RN (2001) AC conductivity and magneto-electric effect in MnFe_{1.8}Cr_{0.2}O₄–BaTiO₃ composites. *Mater Sci Eng B* 87:53–58. [https://doi.org/10.1016/S0921-5107\(01\)00695-X](https://doi.org/10.1016/S0921-5107(01)00695-X)
48. Idrees M, Nadeem M, Atif M, Siddique M, Mehmood M, Hassan MM (2011) Origin of colossal dielectric response in LaFeO₃. *Acta Mater* 59:1338–1345. <https://doi.org/10.1016/j.actamat.2010.10.066>
49. Vishwanathan B, Murthy VRK (1990) Ferrite materials: science and technology. In: *Ferrite materials*. Narosa Publishing House, New Delhi, p 6
50. Maxwell JC (1892) *A treatise on electricity and magnetism*, 3rd edn. Clarendon press, Oxford
51. Wagner KW (1914) Explanation of the dielectric after-effect processes on the basis of Maxwell's ideas. *Arch Elektrotech* 2:371–387. <https://doi.org/10.1007/BF01657322>
52. Wagner KW (1913) The distribution of relaxation times in typical dielectrics. *Ann Phys* 40:817–855
53. Himansh AK, Ray DK, Sinha TP (2005) Ac conductivity of conducting polymer prepared with the use of water soluble support polymer. *Indian J Phys* 79:1049–1052. <https://192.168.1.41:8080/xmlui/handle/123456789/2292>
54. Matteeva ES (1996) Residual water as a factor influencing the electrical properties of polyaniline. The role of hydrogen bonding of the polymer with solvent molecules in the formation of a conductive polymeric network. *Synth Met* 79:127–139. [https://doi.org/10.1016/0379-6779\(96\)80180-9](https://doi.org/10.1016/0379-6779(96)80180-9)
55. Bhat S, Khosa SK, Kotru PN, Tandon RP (1995) Dielectric studies of lanthanum heptamolybdate crystals grown from gels. *Mater Sci Eng B* 309:7–11. [https://doi.org/10.1016/0921-5107\(94\)01129-x](https://doi.org/10.1016/0921-5107(94)01129-x)
56. Mantas PQ (1999) Dielectric response of materials: extension to the debye model. *J Eur Ceram Soc* 19:2079–2086. [https://doi.org/10.1016/S0955-2219\(98\)00273-8](https://doi.org/10.1016/S0955-2219(98)00273-8)
57. Tonks DL, Silver RN (1982) Small-polaron models for the hydrogen-concentration dependence of hydrogen diffusion in Nb. *Phys Rev B* 26(12):6455–6469. <https://doi.org/10.1103/PhysRevB.26.6455>
58. Ghosh A (1990) ac conduction in iron bismuthate glassy semiconductors. *Phys Rev B* 42(2):1388–1393. <https://doi.org/10.1103/PhysRevB.42.1388>
59. Pike GE (1972) ac conductivity of scandium oxide and a new hopping model for conductivity. *Phys Rev B* 6(4):1572–1580. <https://doi.org/10.1103/PhysRevB.6.1572>

60. Jonscher AK (1977) The ‘universal’ dielectric response. *Nature* 267:673–679. <https://doi.org/10.1038/267673a0>
61. Long AR (1982) Frequency-dependent loss in amorphous semiconductors. *Adv Phys* 31:553–637. <https://doi.org/10.1080/00018738200101418>
62. Farid AM, Atyia HE, Hegab NA (2005) AC conductivity and dielectric properties of Sb₂Te₃ thin films. *Vacuum* 80:284–294. <https://doi.org/10.1016/j.vacuum.2005.05.003>
63. Elliott SR (1978) Temperature dependence of a.c. conductivity of chalcogenide glasses. *Philos Mag B* 37:553–560. <https://doi.org/10.1080/01418637808226448>
64. Street RA, Mott NF (1975) States in the gap in glassy semiconductors. *Phys Rev Lett* 35:1293–1296. <https://doi.org/10.1103/PhysRevLett.35.1293>
65. Shimakawa K (1982) On the temperature dependence of a.c. conduction in chalcogenide glasses. *Philos Mag B* 46:123–135. <https://doi.org/10.1080/13642818208246429>
66. Rockstad HK (1969) Evidence for hopping conduction in amorphous chalcogenide films. *Solid State Commun* 7:1507–1509. [https://doi.org/10.1016/0038-1098\(69\)90031-3](https://doi.org/10.1016/0038-1098(69)90031-3)
67. Rockstad HK (1971) Comments on the a.c. conductivity of amorphous chalcogenides. *Solid State Commun* 9:2233–2237. [https://doi.org/10.1016/0038-1098\(71\)90637-5](https://doi.org/10.1016/0038-1098(71)90637-5)

Publisher’s Note Springer Nature remains neutral with regard to jurisdictional claims in published maps and institutional affiliations.

Authors and Affiliations

Nadeem Anwar¹  · Abdul Shakoor¹ · Niaz Ahmad Niaz¹ · Ghulam Ali² · Muhammad Qasim¹ · Muhammad Irfan¹ · Arshad Mahmood³

✉ Nadeem Anwar
nadeemgcc182@gmail.com

¹ Department of Physics, Bahauddin Zakariya University, Multan 60800, Pakistan

² U.S.-Pakistan Center for Advanced Studies in Energy(USPCAS-E), National University of Science and Technology (NUST), Islamabad 44000, Pakistan

³ National Institute of Laser and Optronics (NILOP), Islamabad, Pakistan